Copyright © 2012 Tech Science Press CMC, vol.30, no.2, pp.145-176, 2012

A Three-Dimensional Model of Shape Memory Alloys under Coupled Transformation and Plastic Deformation

B. Chen[1,2], X. Peng[1,2,3], X. Chen[1,2], J. Wang[4], H. Wang[4] and N. Hu[1,5,6]

Abstract: A three-dimensional phenomenological model for coupled transformation and plastic behavior of shape memory alloys (SMAs) is presented. The strain is separated into elastic, thermal, transformation and plastic strain parts, and two yield functions are adopted to describe respectively the transformation and plastic deformation. An integral algorithm is suggested, including the update of the stress and the tangent stiffness. Numerical examples and the comparison with experimental results show that the proposed approach can well describe the behavior of the SMAs subjected to complicated thermal-mechanical loading, demonstrating the validity of the model in the description of the constitutive behavior of SMAs, including shape memory effect, pseudoelasticity, coupled transformation and plastic deformation, and effect of plastic deformation on the inverse transformation, etc. The corresponding user material subroutine UMAT is developed and embedded into FE code ABAQUS, with which the installation process of SMA pipe joints is simulated and the residual contact pressure between connected pipes and the joint is predicted.

Keywords: shape memory alloys, transformation, plastic deformation, constitutive model

1 Introduction

The remarkable properties of shape memory alloys (SMAs) have been receiving increasing attention due to the successful and potential applications in many fields, such as aerospace, medical, and petroleum industries, etc. As a consequence,

[1] Department of Engineering Mechanics, Chongqing University, Chongqing, China
[2] State Key Laboratory of Coal Mine Disaster Dynamics and Control, Chongqing University, Chongqing 400044, China
[3] Corresponding author: X. Peng, *Email address*: xhpeng@cqu.edu.cn
[4] Academy of Engineering Physics, Mianyang, Sichuan, 621900, China
[5] Department of Mechanical Engineering, Chiba University, Chiba, Japan
[6] Corresponding author: Ning Hu, *E-mail address*: huning@faculty.chiba-u.jp

the interest in the research of the thermal-mechanical behavior of SMAs was also rapidly growing.

Significant progresses have been made in constitutive modeling of SMAs since 1990s. The models can generally be categorized as microscopic, micro-macro and phenomenological ones. In the microscopic and micro-macro models, micromechanics is often combined with continuum mechanics for the description of the macroscopic behavior of SMAs [Sun and Hwang(1993a,b); Lexcellent et al.(1996); Siredey et al.(1999); Gao et al.(2000a,b); Peng et al.(2001); Blanc and Lexcellent (2004); Patoor et al.(2006); Lagoudas et al.(2006); Liu et al.(2011); Kang et al.(2010)]. These models are useful for understanding the fundamental features at micro-level, but most of them are not easily applied in the analysis of practical engineering problems. The phenomenological models [Boyd and Lagoudas (1996); Auricchio et al.(1997); Raniecki and Lexcellent (1998)] are usually based on continuum thermodynamics with internal state variables taking into account the effects of the changes in microstructures. These models can, in general, be applied efficiently to predict the behavior of SMA components and devices.

In the phenomenological models, the behavior of SMAs is often described with strain, stress, temperature, entropy and internal variables that are often introduced to describe the change in internal structures. If the behavior of an SMA involves mainly elasticity and phase transformation, the typical internal state variables used are the martensite volume fraction and macroscopic transformation strain, respectively. Correspondingly, the models with internal variables can further be classified into two groups. In one group, the martensite volume fraction, ξ, is taken as an internal variable, and the transformation kinetics, i.e., the evolution of ξ is assumed to be related to the current temperature and macroscopic stress state. Tanaka et al. (1995) proposed a set of exponential functions to describe respectively the forward and inverse transformations by making use of the von-Mises equivalent stress and temperature. Liang and Rogers (1990) suggested an evolution of ξ with cosine functions. Brinson et al. (1993) suggested a different method to describe the transformation kinetics, in which ξ is divided into two parts, determined by temperature and stress respectively. Peng et al. (2001) proposed a model for SMAs with the concept that an SMA is composed of austenite and martensite and its constitutive behavior is the combination of the individual behavior of each of the two phases, in which Tanaka's transformation kinetics rule was adopted.

The models in the other group were usually developed within the framework of thermodynamics. Constitutive equations were mainly specified as two parts: state equations for the entities conjugating the control variables, and kinetic equations for the internal variables. The state equations can be obtained directly or formulated by the partial derivative of a free energy function in the sense of the Clausius–

Duhem inequality. The kinetic equations of internal variables often depend on the equations relating the rates of the internal variables to the current state and its time derivatives. Leclercq and Lexcellent (1996) proposed a model in the framework of irreversible thermodynamics with internal variables, in which a specific free energy function and two internal variables were introduced. The two variables were defined as the volume fraction of self-accommodation (pure thermal effect) and oriented (stress-induced) product phase. Popov and Lagoudas (2007) presented a model that could take into account both the direct conversion of austenite into detwinned martensite and the detwinning of self-accommodated martensite. In the model by Bo and Lagoudas (1999a, b, c) and Lagoudas et al. (1999), the increments of both the elastic potential and the Gibbs chemical energy over a representative volume element (RVE) with respect to an infinitesimal increment of martensite were introduced, and a set of internal variables, including the martensite volume fraction, the macroscopic transformation strain, the back stress and the drag stress due to both martensitic transformation and its interaction with plastic strain were adopted. Panico and Brinson (2007) also proposed a model in the framework of the classical irreversible thermodynamics, which could take into account the effect of multiaxial stress states and non-proportional loading histories, and account for the evolution of both twinned and detwinned martensite. The model by Helm and Haupt (2003) is based on a free energy function and the evolution of internal state variables, in which the energy stored during a thermal-mechanical process could be considered. The model proposed by Souza et al. (1998) can capture both shape memory effect (SME) and pseudoelasticity (PE) in a small strain regime, and the macroscopic kinetics of stress-induced phase transformations could be described with a transformation strain tensor. Auricchio and Petrini (2002) discussed some improvements to the model by Souza et al. (1998), developed the corresponding integration algorithm, and discussed some typical aspects in SMA modeling, such as asymmetry of tension and compression permanent inelasticity, as well as different independent internal variables [Auricchio et al.(2004a,b, 2007, 2010)]. Zaki and Moumni (2007) developed a model for the behavior of SMAs under cyclic loading, in which three new state variables, internal stress, residual strain and cumulated martensite volume fraction, were introduced.

In practical application, stress concentration may inevitably exist, which may induce local plastic deformation. Under complex loading, the interaction between irreversible plastic strain and recoverable transformation strain should be considered. Zhao and Zhang (1992) found that in SMA $Ni_{47}Ti_{44}Nb_9$ there exists a characteristic deformation temperature (M_s+30°C) and a critical strain range (16%), at which deformation can effectively increase the inverse transformation temperature and transformation hysteretic loop. In order to explain this phenomenon, Piao et al

(1993) investigated the transformation behavior of several SMAs, and speculated that the elastic strain energy stored during the forward transformation might be relaxed by plastic deformation. As a result, the inverse transformation temperature, such as A_s and A_f, could be increased. Casciati et al. (2011) investigated the fatigue characteristics of multigrain samples of a specific Cu-based alloy under several loading-unloading cycles with different strain amplitude. Some researchers [Paiva et al.(2005); Patoor et al.(2009); Lagoudas et al.(2009, 2010); Zaki et al.(2007)] investigated the residual irreversible strain during martensitic deformation. Peng et al. (2012) developed a dual-phase mixture model for the constitutive behavior of shape memory alloys, involving coupled transformation, reorientation and plastic deformation. Although this coupling between transformation and plastic deformation may contain some important information for the extension of the application of SMAs, the model involving plastic strain that occurs after transformation and its effect on the following inverse transformation has not yet been sufficiently investigated, especially for the urgent need of engineering applications.

Inspired by the theories of Souza et al.(1998) and Auricchio and Petrini (2002), we intend to establish a unified model for the description of SME and PE, taking into account the effects of plastic deformation, as well as its interaction with transformation. In Section 2 the governing equations are obtained based on the given assumptions; in Section 3 the incremental form of the governing equations are derived. The integration algorithm of the model is developed in Section 3; and Section 4 is devoted to the numerical simulation and the comparison with experimental results. At the end of Section 4, the proposed constitutive model and the numerical approach are applied to the simulation of a pipe joint assembly progress; the conclusion and discussion are given in Section 5.

2 3-D modeling of SMAs considering effect of plastic strain

The modeling of the SMAs treated in this work starts from the assumption that the free energy is the function of elastic strain $\boldsymbol{\varepsilon}^e$, transformation strain $\boldsymbol{\varepsilon}^t$, tensor $\boldsymbol{\alpha}$ and accumulated plastic strain p associated with plasticity-induced hardening, and temperature T (Lemaitre and Chaboche, 1990), i.e.,

$$\Phi = \Phi(\boldsymbol{\varepsilon}^e, \quad \boldsymbol{\varepsilon}^t, \quad \boldsymbol{\alpha}, \quad p, \quad T), \tag{1}$$

where

$$\boldsymbol{\varepsilon}^e = \boldsymbol{\varepsilon} - \varepsilon^t - \boldsymbol{\varepsilon}^p - \boldsymbol{\varepsilon}^\theta, \tag{2}$$

$\boldsymbol{\varepsilon}$ and $\boldsymbol{\varepsilon}^p$ are total strain and plastic strain, respectively, and $\boldsymbol{\varepsilon}^\theta = \theta(T - T_0)$ is thermal strain, $\boldsymbol{\theta}$ is the coefficient tensor of thermal expansion and T_0 is a reference temperature. Φ can further be expressed as the sum of the contributions from elastic, transformation and plastic deformation as well as temperature, taking into account the interaction between transformation and plasticity,

$$\Phi(\boldsymbol{\varepsilon}^e,\boldsymbol{\varepsilon}^t,\boldsymbol{\alpha},p,T)=\Phi^e(\boldsymbol{\varepsilon}^e,T)+\Phi^t(\boldsymbol{\varepsilon}^t,T)+\Phi^p(\boldsymbol{\alpha},p,T)+\Phi^\theta(T)+\Phi^c(\boldsymbol{\varepsilon}^t,p), \quad (3)$$

where $\Phi^e(\boldsymbol{\varepsilon}^e,T)=\frac{1}{2\rho}\boldsymbol{\varepsilon}^e:\mathbf{C}:\boldsymbol{\varepsilon}^e$,

$$\Phi^t(\boldsymbol{\varepsilon}^t,T)=\frac{1}{3\rho}C^t\varepsilon^t:\boldsymbol{\varepsilon}^t+\frac{1}{\rho}\tau_M(T)\left\|\boldsymbol{\varepsilon}^t\right\|+\frac{1}{\rho}\Gamma(\boldsymbol{\varepsilon}^t),$$

$$\Phi^p(\boldsymbol{\alpha},p,T)=\frac{1}{3\rho}C^p\alpha:\boldsymbol{\alpha}+\frac{1}{\rho}Y(p),$$

$$\Phi^\theta(T)=c_v[(T-T_0)-T\ln(\frac{T}{T_0})],$$

$$\Phi^c(\boldsymbol{\varepsilon}^t,p)=-\frac{1}{\rho}Q(p)\left\|\boldsymbol{\varepsilon}^t\right\|,$$

$\mathbf{C}$ is the standard isotropic elasticity tensor, C^p and C^t are material parameters, ρ and c_v are density and specific heat, respectively, which are assumed invariant during phase change, $\|\bullet\|$ denotes the Euclidean norm of an arbitrary tensor "$\bullet$" of rank two, $\tau_M(T)$ is defined as

$$\tau_M(T)=\begin{cases}\mathrm{B}(T-M_0) & \text{if } T>M_0\\ 0 & \text{if } T\le M_0\end{cases}, \quad (4)$$

where the parameter B represents the sensitivity of the stress with respect to temperature T, and M_0 is the reference temperature below which no twinned martensite is observed (Souza et al., 1998), and $\Gamma(\boldsymbol{\varepsilon}^t)$ as well as $\boldsymbol{\varepsilon}^t$ satisfies the following phenomenological physical constraints

$$\begin{aligned}&\gamma\ge 0,\\&\left\|\boldsymbol{\varepsilon}^t\right\|-\varepsilon_L\le 0,\\&\Gamma(\boldsymbol{\varepsilon}^t)=\gamma(\left\|\boldsymbol{\varepsilon}^t\right\|-\varepsilon_L)=0,\end{aligned} \quad (5)$$

in which γ is a Lagrange multiplier, ε_L is related to the saturated state of phase transformation. The function of $\Gamma(\boldsymbol{\varepsilon}^t)$ is similar to the additional indicator function adopted by Souza et al. (1998) and Frémond et al. (1987, 1996) for the saturated phase transformations. $Y(p)$ and $Q(p)$ will be specified later.

Making using of the derivative of Equation (3) with respect to time

$$\dot{\Phi} = \frac{\partial \Phi}{\partial \boldsymbol{\varepsilon}^e} : \dot{\boldsymbol{\varepsilon}}^e + \frac{\partial \Phi}{\partial T}\dot{T} + \frac{\partial \Phi}{\partial \boldsymbol{\varepsilon}^t} : \dot{\boldsymbol{\varepsilon}}^t + \frac{\partial \Phi}{\partial \boldsymbol{\alpha}} : \dot{\boldsymbol{\alpha}} + \frac{\partial \Phi}{\partial p}\dot{p}, \tag{6}$$

and the Clausius–Duhem inequality [Lemaitre and Chaboche (1990)],

$$\boldsymbol{\sigma} : \dot{\boldsymbol{\varepsilon}} - \rho(\dot{\Phi} + \eta \dot{T}) \geq 0 \tag{7}$$

one obtains

$$\begin{aligned} \boldsymbol{\sigma} : \dot{\boldsymbol{\varepsilon}} - \rho(\dot{\Phi} + \eta \dot{T}) &= (\boldsymbol{\sigma} - \rho \frac{\partial \Phi}{\partial \boldsymbol{\varepsilon}^e})\dot{\boldsymbol{\varepsilon}}^e + \rho(-\eta - \frac{\partial \Phi}{\partial T} + \frac{1}{\rho}\boldsymbol{\sigma} : \boldsymbol{\theta})\dot{T} \\ &+ \boldsymbol{\sigma} : \dot{\boldsymbol{\varepsilon}}^t + \boldsymbol{\sigma} : \dot{\boldsymbol{\varepsilon}}^p - \rho \frac{\partial \Phi}{\partial \boldsymbol{\varepsilon}^t} : \dot{\boldsymbol{\varepsilon}}^t - \rho \frac{\partial \Phi}{\partial \boldsymbol{\alpha}} : \dot{\boldsymbol{\alpha}} - \frac{\partial \Phi}{\partial p}\dot{p} \geq 0. \end{aligned} \tag{8}$$

It implies a general elasticity law of the form

$$\boldsymbol{\sigma} = \rho \frac{\partial \Phi}{\partial \boldsymbol{\varepsilon}^e} = \mathbf{C} : (\boldsymbol{\varepsilon} - \boldsymbol{\varepsilon}^t - \boldsymbol{\varepsilon}^p - \boldsymbol{\varepsilon}^\theta) \tag{9}$$

and

$$\eta = -\frac{\partial \Phi}{\partial T} + \frac{1}{\rho}\boldsymbol{\sigma} : \boldsymbol{\theta} = c_v \ln(\frac{T}{T_0}) - \frac{1}{\rho}\mathrm{B}\left\|\boldsymbol{\varepsilon}^t\right\| + \frac{1}{\rho}\boldsymbol{\sigma} : \boldsymbol{\theta}. \tag{10}$$

where $\boldsymbol{\sigma}$ and η are stress and entropy, respectively. From Equation (3) we get following two stress-like counterparts

$$\boldsymbol{\chi}^t = \rho \frac{\partial \Phi}{\partial \boldsymbol{\varepsilon}^t} = \frac{2}{3}C^t \boldsymbol{\varepsilon}^t + (\tau_M(T) - Q(p) + \gamma)\mathbf{N}^{\boldsymbol{\varepsilon}^t} \tag{11}$$

and

$$\boldsymbol{\chi}^p = \rho \frac{\partial \Phi}{\partial \boldsymbol{\alpha}} = \frac{2}{3}C^p \boldsymbol{\alpha} \tag{12}$$

where $\boldsymbol{\chi}^t$ and $\boldsymbol{\chi}^p$ can be regarded as transformation back stress and plastic back stress, respectively. The direction of $\boldsymbol{\varepsilon}^t$ is defined as

$$\mathbf{N}^{\boldsymbol{\varepsilon}^t} = \boldsymbol{\varepsilon}^t / \left\|\boldsymbol{\varepsilon}^t\right\|. \tag{13}$$

Since $\|\boldsymbol{\varepsilon}^t\| = 0$ as $\boldsymbol{\varepsilon}^t = 0$, $\overline{\|\boldsymbol{\varepsilon}^t\|} = \sqrt{\|\boldsymbol{\varepsilon}^t\|^2 + \delta} - \sqrt{\delta}$ is defined to replace the $\|\boldsymbol{\varepsilon}^t\|$ in the denominator on the RHS of Eq. (13) to avoid singularity [Auricchio et al. (2010)], where δ is a user-defined small positive number. The function $Q(p)$ affects directly the occurrence of transformation. We define $Q(p) = Q_0(1-\exp(-\xi p))$based on the fact that there is a close relation between the inverse transformation start temperature A_s and the permanent strain [Piao et al. (1993)], where Q_0 and ξ are the material parameters. Bo and Lagoudas (1999b) used this form of the equation to describe the phenomenon that plastic deformation increases continuously, and the overall effect of the dislocations on the phase transformation will reach a certain limit. Then the following drag stress of plastic is defined as

$$R = \rho\frac{\partial\Phi}{\partial p} = Y'(p) - Q'(p)\left\|\boldsymbol{\varepsilon}^t\right\| = R_0\left(1-\exp\left(-\zeta p\right)\right) - Y_0\exp\left(-\xi p\right)\left\|\boldsymbol{\varepsilon}^t\right\|, \quad (14)$$

whereR_0, ζ and Y_0 are the material parameters. The first term on the RHS of Equation (14) is often used to describe the plastic deformation induced isotopic hardening [Lemaitre and Chaboche (1990)], and the last term on the RHS of the equation is an additional term related to the coupling of transformation and plastic deformation.

Using Equations (8) $\sim$ (14), we obtain

$$\boldsymbol{\sigma} : \dot{\boldsymbol{\varepsilon}}^t + \boldsymbol{\sigma} : \dot{\boldsymbol{\varepsilon}}^p - \boldsymbol{\chi}^t : \dot{\boldsymbol{\varepsilon}}^t - \boldsymbol{\chi}^p : \dot{\boldsymbol{\alpha}} - R\dot{p} \geq 0. \quad (15)$$

In order to derive the evolution of the internal variables,$\boldsymbol{\varepsilon}^t, \boldsymbol{\varepsilon}^p, \boldsymbol{\alpha}andp$, the concept of dissipation potential and the rule of normality are adopted [Lemaitre and Chaboche (1990)],

$$\varphi = \boldsymbol{\sigma} : \dot{\boldsymbol{\varepsilon}}^t + \boldsymbol{\sigma} : \dot{\boldsymbol{\varepsilon}}^p - \boldsymbol{\chi}^t : \dot{\boldsymbol{\varepsilon}}^t - \boldsymbol{\chi}^p : \dot{\boldsymbol{\alpha}} - R\dot{p}. \quad (16)$$

Making use of the Legendre-Fenchel transformation that enables to define the corresponding potential $\Psi(\boldsymbol{\sigma}, \boldsymbol{\chi}^t, \boldsymbol{\chi}^p, R, T)$ [Lemaitre and Chaboche (1990)], we introduce the following two dissipation potential functions

$$\Psi^t(\boldsymbol{\sigma}, \boldsymbol{\chi}^t, T) = f^t(\boldsymbol{\sigma}, \boldsymbol{\chi}^t, T) \quad (17)$$

and

$$\Psi^p(\boldsymbol{\sigma}, \boldsymbol{\chi}^p, R, T) = f^p(\boldsymbol{\sigma}, \boldsymbol{\chi}^p, R, T) + \frac{3}{4}\frac{a}{C^p}\boldsymbol{\chi}^p : \boldsymbol{\chi}^p \quad (18)$$

to describe respectively the evolution of the internal variables for transformation and plastic, where a is a parameter, $f^t(\boldsymbol{\sigma}, \boldsymbol{\chi}^t, T)$ and $f^p(\boldsymbol{\sigma}, \boldsymbol{\chi}^p, R, T)$ are the yield functions of transformation and plastic deformation, respectively, and are defined as

$$f^t(\boldsymbol{\sigma},\boldsymbol{\chi}^t,T) = J_2(\boldsymbol{\sigma}' - \boldsymbol{\chi}^t) - \sigma_s^t, \tag{19}$$

and

$$f^p(\boldsymbol{\sigma},\boldsymbol{\chi}^p,R,T) = J_2(\boldsymbol{\sigma}' - \boldsymbol{\chi}^p) - R - \sigma_s^p, \tag{20}$$

where σ_s^t and σ_s^p are related to the yield of transformation and plastic deformation,

$$J_2(\boldsymbol{\beta}) = \sqrt{\frac{3}{2}\boldsymbol{\beta} : \boldsymbol{\beta}} \tag{21}$$

$\boldsymbol{\beta}$ is an arbitrary tensor of rank two. The evolution equations of $\boldsymbol{\varepsilon}^t, \boldsymbol{\varepsilon}^p, \boldsymbol{\alpha}$ and p can be obtained as

$$\dot{\boldsymbol{\varepsilon}}^t = -\dot{\lambda}^t \frac{\partial \Psi^t}{\partial \boldsymbol{\chi}^t} = \dot{\lambda}^t \frac{\partial \Psi^t}{\partial \boldsymbol{\sigma}} = \frac{3}{2} \frac{\boldsymbol{\sigma}' - \boldsymbol{\chi}^\mathbf{t}}{J_2(\boldsymbol{\sigma}' - \boldsymbol{\chi}^t)} \dot{\lambda}^t = \mathbf{N}^t(\boldsymbol{\sigma},\boldsymbol{\chi}^t)\dot{\lambda}^t \tag{22}$$

$$\dot{\boldsymbol{\varepsilon}}^p = \dot{\lambda}^p \frac{\partial \Psi^p}{\partial \boldsymbol{\sigma}} = \frac{3}{2} \frac{\boldsymbol{\sigma}' - \boldsymbol{\chi}^p}{J_2(\boldsymbol{\sigma}'} - \boldsymbol{\chi}^p)\dot{\lambda}^p = \mathbf{N}^p(\boldsymbol{\sigma},\boldsymbol{\chi}^p)\dot{\lambda}^p \tag{23}$$

$$\dot{\boldsymbol{\alpha}} = -\dot{\lambda}^p \frac{\partial \Psi^p}{\partial \boldsymbol{\chi}^p} = \frac{3}{2} \frac{\boldsymbol{\sigma}' - \boldsymbol{\chi}^p}{J_2(\boldsymbol{\sigma}'} - \boldsymbol{\chi}^p)\dot{\lambda}^p - \frac{3}{2}\frac{a}{C^p}\boldsymbol{\chi}^p\dot{\lambda}^p = \mathbf{H}^p(\boldsymbol{\sigma},\boldsymbol{\chi}^p)\dot{\lambda}^p \tag{24}$$

$$\dot{p} = -\dot{\lambda}^p \frac{\partial \Psi^p}{\partial R} = \dot{\lambda}^p \tag{25}$$

where$\dot{\lambda}^p = \sqrt{(2/3)\dot{\boldsymbol{\varepsilon}}^p : \dot{\boldsymbol{\varepsilon}}^p}and\dot{\lambda}^t = \sqrt{(2/3)\dot{\boldsymbol{\varepsilon}}^t : \dot{\boldsymbol{\varepsilon}}^t}$. Using Equations (22∼25), the Clausius–Duhem inequality can be further specified as

$$\dot{\lambda}^t\left(\frac{\partial \Psi^t}{\partial \boldsymbol{\sigma}} : \boldsymbol{\sigma} + \frac{\partial \Psi^t}{\partial \boldsymbol{\chi}^t} : \boldsymbol{\chi}^t\right) + \dot{\lambda}^p\left(\frac{\partial \Psi^p}{\partial \boldsymbol{\sigma}} : \boldsymbol{\sigma} + \frac{\partial \Psi^p}{\partial \boldsymbol{\chi}^p} : \boldsymbol{\chi}^p + \frac{\partial \Psi^p}{\partial \mathrm{R}}\mathrm{R}\right) \geq 0 \tag{26}$$

It is easy to prove that inequality (26) holds if the following conditions are satisfied

1. Ψ^t and Ψ^p are convex, while $f^t = 0$ and $f^p = 0$,
2. $\Psi^t(\mathbf{0},\mathbf{0},T) = 0$ and $\Psi^p(\mathbf{0},\mathbf{0},0,T) = 0$, while $f^t = 0$ and $f^p = 0$.

Obviously, Equations (17) and (18) satisfy the above conditions, therefore, Inequality (26) is always satisfied with the evolution of $\boldsymbol{\varepsilon}^t, \boldsymbol{\varepsilon}^p, \boldsymbol{\alpha}$ and p defined in Equations (22) ∼ (25). From several argumentations on the evolution laws and on the nucleation criteria of transformation and plastic deformation, it is possible to conclude that material can be either in elastic state, pure phase transformation, pure saturated transformation state, or plastic deformation occurring simultaneously with the previous several states.

3 Incremental constitutive equations

3.1 Return mapping schemes

For the incremental analysis of the material response, we replace all the rate quantities in Equations (22) $\sim$ (25) with the corresponding increments within the interval considered. Suppose the analysis for the nth increment of loading has been finished, the values of $\boldsymbol{\varepsilon}_n^e, \boldsymbol{\varepsilon}_n^t, \boldsymbol{\varepsilon}_n^p, \boldsymbol{\alpha}_n, p_n$ and γ_n, and the yielding functions $f^t(\boldsymbol{\sigma}, \boldsymbol{\chi}^t, T)$ and $f^p(\boldsymbol{\sigma}, \boldsymbol{\chi}^p, R, T)$, the kinematic hardening function $\mathbf{H}^p(\boldsymbol{\sigma}, \boldsymbol{\chi}^p)$, and the flow directions $\mathbf{N}^t(\boldsymbol{\sigma}, \boldsymbol{\chi}^t)$ and $\mathbf{N}^p(\boldsymbol{\sigma}, \boldsymbol{\chi}^p)$ at the instant t_n have been obtained. Given the increments ΔT and $\Delta \boldsymbol{\varepsilon}$ applied in time interval $[t_n, t_{n+1}]$, $\boldsymbol{\varepsilon}_{n+1}^e, \boldsymbol{\varepsilon}_{n+1}^t, \boldsymbol{\varepsilon}_{n+1}^p, \boldsymbol{\alpha}_{n+1}, p_{n+1}$ and γ_{n+1} at the instant t_{n+1} can be obtained by solving the following algebraic equations associated with Equations (11) $\sim$ (13)

$$\boldsymbol{\varepsilon}_{n+1}^e = \boldsymbol{\varepsilon}_{n+1}^{e\,trial} - \Delta\lambda^t \mathbf{N}^t(\boldsymbol{\sigma}_{n+1}, \boldsymbol{\chi}_{n+1}^t) - \Delta\lambda^p \mathbf{N}^p(\boldsymbol{\sigma}_{n+1}, \boldsymbol{\chi}_{n+1}^p), \tag{27}$$

$$\boldsymbol{\varepsilon}_{n+1}^t = \boldsymbol{\varepsilon}_n^t + \Delta\lambda^t \mathbf{N}^t(\boldsymbol{\sigma}_{n+1}, \boldsymbol{\chi}_{n+1}^t), \tag{28}$$

$$\boldsymbol{\varepsilon}_{n+1}^p = \boldsymbol{\varepsilon}_n^p + \Delta\lambda^p \mathbf{N}^p(\boldsymbol{\sigma}_{n+1}, \boldsymbol{\chi}_{n+1}^p), \tag{29}$$

$$\boldsymbol{\alpha}_{n+1}^p = \boldsymbol{\alpha}_n^p + \Delta\lambda^p \mathbf{H}^p(\boldsymbol{\sigma}_{n+1}, \boldsymbol{\chi}_{n+1}^p), \tag{30}$$

subjected to the following constrains

$$\Delta\lambda^t \geq 0, \quad f^t(\boldsymbol{\sigma}_{n+1}, \boldsymbol{\chi}_{n+1}^t, T) \leq 0, \quad \Delta\lambda^t f^t(\boldsymbol{\sigma}_{n+1}, \boldsymbol{\chi}_{n+1}^t, T) = 0, \tag{31}$$

$$\Delta\lambda^p \geq 0, \quad f^p(\boldsymbol{\sigma}_{n+1}, \boldsymbol{\chi}_{n+1}^p, R_{n+1}, T) \leq 0, \quad \Delta\lambda^p f^p(\boldsymbol{\sigma}_{n+1}, \boldsymbol{\chi}_{n+1}^p, R_{n+1}, T) = 0, \tag{32}$$

$$\gamma \geq 0, \quad \left\|\boldsymbol{\varepsilon}_{n+1}^t\right\| - \varepsilon_L \leq 0, \quad \gamma\left(\left\|\boldsymbol{\varepsilon}_{n+1}^t\right\| - \varepsilon_L\right) = 0, \tag{33}$$

where $\boldsymbol{\varepsilon}_{n+1}^{etrial} = \boldsymbol{\varepsilon}_n^e + \Delta\boldsymbol{\varepsilon}$. $\boldsymbol{\varepsilon}_{n+1}^{etrial}$ is computed by assuming that the material is elastic during the interval (correspondingly,$\boldsymbol{\varepsilon}_{n+1}^{ttrial} = \boldsymbol{\varepsilon}_n^t, \boldsymbol{\alpha}_{n+1}^{trial} = \boldsymbol{\alpha}_n, p_{n+1}^{trial} = p_n$). The corresponding stress and the back stress can be called elastic trial stress and elastic trial back stress, given by

$$\boldsymbol{\sigma}_{n+1}^{trial} = \mathbf{C} : \boldsymbol{\varepsilon}_{n+1}^{etrial}, \tag{34}$$

$$\boldsymbol{\chi}_{n+1}^{t\,trial} = \frac{2}{3} C^t \boldsymbol{\varepsilon}_{n+1}^{t\,trial} + (\tau_M(T) - Q(p_{n+1}^{trial}) + \gamma)\mathbf{N}^{\boldsymbol{\varepsilon}^t}, \tag{35}$$

$$\boldsymbol{\chi}_{n+1}^{p\,trial} = \frac{2}{3} C^p \boldsymbol{\alpha}_{n+1}^{trial}, \tag{36}$$

and

$$R_{n+1}^{trial} = R_0(1 - \exp(-\zeta p_{n+1}^{trial})) - Y_0 \exp(-\xi p_{n+1}^{trial}) \left\|\boldsymbol{\varepsilon}_{n+1}^{t\,trial}\right\| \tag{37}$$

Based on the above results, the two limit functions can be computed. If

$$f^t(\boldsymbol{\sigma}_{n+1}^{t\,trial}, \boldsymbol{\chi}_{n+1}^{t\,trial}, T) \leq 0$$

and

$$f^p(\boldsymbol{\sigma}_{n+1}^{p\,trial}, \boldsymbol{\chi}_{n+1}^{p\,trial}, R_{n+1}^{trial}, T) \leq 0 \tag{38}$$

i.e., the elastic trail stress lies within the elastic domain or on the yield surface, then the material response should be elastic and the trail stress $\boldsymbol{\sigma}_{n+1}^{trial}$ as well as the internal variables takes the updated ones. Otherwise, an inelastic correction for the material response will be performed using a Newton-Raphson iteration scheme. For the material state discussed in Section 2, we can define a set of equations

$$\{\mathbf{f}(\mathbf{x})\} = \{\mathbf{0}\} \tag{39}$$

for the unknown $\{\mathbf{x}\}$. For example, if the material is in the state of saturated phase transformation and plastic deformation occurs simultaneously, the yield functions of transformation and plasticity and Lagrangian constraint function $\Gamma(\boldsymbol{\varepsilon}^t)$ will be equal to zero. The unknown quantity is $\{\mathbf{x}\} = \left(\boldsymbol{\sigma}_{n+1}, \boldsymbol{\chi}_{n+1}^t, \boldsymbol{\chi}_{n+1}^p, \Delta\lambda^t, \Delta\lambda^p, \gamma_{n+1}\right)^{\mathrm{T}}$, and the following residual equations for the residual parts of these quantities should be satisfied

$$\{\mathbf{f}(\mathbf{x})\} = \left\{ \begin{array}{l} \mathbf{C}^{-1} : \boldsymbol{\sigma}_{n+1} - \boldsymbol{\varepsilon}_{n+1}^{etrial} + \Delta\lambda^t \mathbf{N}_{n+1}^t + \Delta\lambda^p \mathbf{N}_{n+1}^p \\ \boldsymbol{\chi}_{n+1}^t - \frac{2}{3} C^t \boldsymbol{\varepsilon}_{n+1}^t - \left(\tau_M - Q(p_{n+1}) + \gamma_{n+1}\right) \mathbf{N}_{n+1}^{\boldsymbol{\varepsilon}^t} \\ \boldsymbol{\chi}_{n+1}^p - \frac{2}{3} C^p \boldsymbol{\alpha}_{n+1} \\ J_2(\boldsymbol{\sigma}_{n+1}' - \boldsymbol{\chi}_{n+1}^t) - \sigma_s^t \\ J_2(\boldsymbol{\sigma}_{n+1}' - \boldsymbol{\chi}_{n+1}^p) - \mathrm{R}(\mathrm{p}_{n+1}) - \sigma_s^p \\ \left\| \boldsymbol{\varepsilon}_{n+1}^t \right\| - \varepsilon_L \end{array} \right\} = \{\mathbf{0}\}. \tag{40}$$

To solve the unknown quantities$\{\mathbf{x}\}$, the Jacobian matrix is computed:

$$[\mathbf{D}] = \frac{\partial \{\mathbf{f}(\mathbf{x})\}}{\partial \{\mathbf{x}\}} =$$

$$\begin{bmatrix} \mathbf{Q} & \Delta\lambda^t \frac{\partial \mathbf{N}^t}{\partial \boldsymbol{\chi}^t} & \Delta\lambda^p \frac{\partial \mathbf{N}^p}{\partial \boldsymbol{\chi}^p} & \mathbf{N}^t & \mathbf{N}^p & \mathbf{0} \\ -\Delta\lambda^t \mathbf{P} : \frac{\partial \mathbf{N}^t}{\partial \boldsymbol{\sigma}} & \mathbf{I} - \Delta\lambda^t \mathbf{P} : \frac{\partial \mathbf{N}^t}{\partial \boldsymbol{\chi}^t} & \mathbf{0} & -\mathbf{P} : \mathbf{N}^t & Q'(p)\mathbf{N}^{\boldsymbol{\varepsilon}^t} & -\mathbf{N}^{\boldsymbol{\varepsilon}^t} \\ -\frac{2}{3} C^p \Delta\lambda^p \frac{\partial \mathbf{N}^p}{\partial \boldsymbol{\sigma}} & \mathbf{0} & \mathbf{I} - \frac{2}{3} C^p \Delta\lambda^p \frac{\partial \mathbf{H}^p}{\partial \boldsymbol{\chi}^p} & \mathbf{0} & -\frac{2}{3} C^p \mathbf{H}^p & \mathbf{0} \\ \mathbf{N}^t & -\mathbf{N}^t & \mathbf{0} & 0 & 0 & 0 \\ \mathbf{N}^p + m\Delta\lambda^t \frac{\partial \mathbf{N}^t}{\partial \boldsymbol{\sigma}} : \mathbf{N}^{\boldsymbol{\varepsilon}^t} & m\Delta\lambda^t \frac{\partial \mathbf{N}^t}{\partial \boldsymbol{\chi}^t} : \mathbf{N}^{\boldsymbol{\varepsilon}^t} & -\mathbf{N}^p & m\mathbf{N}^{\boldsymbol{\varepsilon}^t} : \mathbf{N}^t & -R'(p) & 0 \\ \Delta\lambda^t \frac{\partial \mathbf{N}^t}{\partial \boldsymbol{\sigma}} : \mathbf{N}^{\boldsymbol{\varepsilon}^t} & \Delta\lambda^t \frac{\partial \mathbf{N}^t}{\partial \boldsymbol{\chi}^t} : \mathbf{N}^{\boldsymbol{\varepsilon}^t} & \mathbf{0} & \mathbf{N}^{\boldsymbol{\varepsilon}^t} : \mathbf{N}^t & 0 & 0 \end{bmatrix} \tag{41}$$

where

$$\frac{\partial \mathbf{N}^t}{\partial \boldsymbol{\chi}^t} = -\frac{3}{2}\frac{1}{J_2(\boldsymbol{\sigma}' - \boldsymbol{\chi}^t)}(\mathbf{I} - \frac{2}{3}\mathbf{N}^t \otimes \mathbf{N}^t), \tag{42}$$

$$\frac{\partial \mathbf{N}^t}{\partial \boldsymbol{\sigma}} = \frac{3}{2}\frac{1}{J_2(\boldsymbol{\sigma}' - \boldsymbol{\chi}^t)}(\mathbf{I}^{dev} - \frac{2}{3}\mathbf{N}^t \otimes \mathbf{N}^t), \tag{43}$$

$$\frac{\partial \mathbf{N}^p}{\partial \boldsymbol{\chi}^p} = -\frac{3}{2}\frac{1}{J_2(\boldsymbol{\sigma}' - \boldsymbol{\chi}^p)}(\mathbf{I} - \frac{2}{3}\mathbf{N}^p \otimes \mathbf{N}^p), \tag{44}$$

$$\frac{\partial \mathbf{N}^p}{\partial \boldsymbol{\sigma}} = \frac{3}{2}\frac{1}{J_2(\boldsymbol{\sigma}' - \boldsymbol{\chi}^p)}(\mathbf{I}^{dev} - \frac{2}{3}\mathbf{N}^p \otimes \mathbf{N}^p), \tag{45}$$

$$\frac{\partial \mathbf{H}^p}{\partial \boldsymbol{\chi}^p} = \frac{\partial \mathbf{N}^p}{\partial \boldsymbol{\chi}^p} - \frac{3}{2}\frac{a}{C^p}\mathbf{I}, \tag{46}$$

$$\mathbf{Q} = \mathbf{C}^{-1} + \Delta\lambda^t \frac{\partial \mathbf{N}^t}{\partial \boldsymbol{\sigma}} + \Delta\lambda^p \frac{\partial \mathbf{N}^p}{\partial \boldsymbol{\sigma}}, \tag{47}$$

$$\mathbf{P} = \frac{2}{3}C^t\mathbf{I} + (\tau_M + \gamma - Q)(\mathbf{I} - \mathbf{N}^{\boldsymbol{\varepsilon}^t} \otimes \mathbf{N}^{\boldsymbol{\varepsilon}^t}) \Big/ \|\boldsymbol{\varepsilon}^t\|, \tag{48}$$

$$m = -Y_0(\exp(-\xi p)), \tag{49}$$

$\mathbf{I}$ and $\mathbf{I}^{dev}$ are the identity tensor and the identity deviatoric tensors of rank four, respectively. In the kth iteration step, Equation (39) can be linearized as

$$[\mathbf{D}]_k \cdot \{\Delta\mathbf{x}\}_k + \{\mathbf{f}(\mathbf{x})\}_k = \{\mathbf{0}\}, \tag{50}$$

from which the unknown$\{\Delta\mathbf{x}\}$ can be solved as

$$\{\Delta\mathbf{x}\}_k = -[\mathbf{D}]_k^{-1} \cdot \{\mathbf{f}(\mathbf{x})\}_k. \tag{51}$$

Staring from the elastic trail, the iteration may continue until $\{\mathbf{f}(\mathbf{x})\} = \{\mathbf{0}\}$ is satisfied within a certain tolerance. Moreover, for each possible case, $\{\mathbf{f}(\mathbf{x})\}$ and $[\mathbf{D}]$ can be obtained by simply removing the corresponding rows and columns according to the constraint conditions for the transformations and plastic deformation.

3.2 Inelastic tangent stiffness tensor

We now address the construction of the inelastic tangent stiffness tensor. Suppose $\boldsymbol{\varepsilon}_n^e, \boldsymbol{\varepsilon}_n^t, \boldsymbol{\varepsilon}_n^p, \boldsymbol{\alpha}_n, p_n$ and $\gamma_n$have been solved and the total strain and temperature, $\boldsymbol{\varepsilon}_{n+1}$ and T_{n+1}, have been prescribed as an input, the stress $\boldsymbol{\sigma}_{n+1}$ can be computed. If we define an algorithmic incremental constitutive function $\boldsymbol{\sigma}_{n+1} = \tilde{\sigma}(\boldsymbol{\varepsilon}_n^t, \boldsymbol{\varepsilon}_n^p, \boldsymbol{\alpha}_n, p_n, \gamma_n, \boldsymbol{\varepsilon}_{n+1})$, the consistent tangent operator can be determined with

$$\mathbf{D}^{in} \equiv \frac{\mathrm{d}\boldsymbol{\sigma}_{n+1}}{\mathrm{d}\boldsymbol{\varepsilon}_{n+1}} = \frac{\partial \tilde{\sigma}_{n+1}}{\partial \boldsymbol{\varepsilon}_{n+1}} \Big|_{\boldsymbol{\varepsilon}_n^t, \boldsymbol{\varepsilon}_n^p, \boldsymbol{\alpha}_n, p_n, \gamma_n} \tag{52}$$

Noticing that $\boldsymbol{\varepsilon}_{n+1}^{etrial} = \boldsymbol{\varepsilon}_{n+1} - \boldsymbol{\varepsilon}_n^t - \boldsymbol{\varepsilon}_n^p - \boldsymbol{\varepsilon}_{n+1}^\theta$, the stress $\boldsymbol{\sigma}_{n+1}$ can also be expressed as

$$\boldsymbol{\sigma}_{n+1} = \bar{\sigma}(\boldsymbol{\varepsilon}_n^t, \boldsymbol{\varepsilon}_n^p, \boldsymbol{\alpha}_n, p_n, \gamma_n, \boldsymbol{\varepsilon}_{n+1}^{e\,trial} + \boldsymbol{\varepsilon}_n^t + \boldsymbol{\varepsilon}_n^p + \boldsymbol{\varepsilon}_{n+1}^\theta), \tag{53}$$

and the consistent tangent operator can be obtained with

$$\mathbf{D}^{in} = \frac{d\tilde{\sigma}_{n+1}}{d\boldsymbol{\varepsilon}_{n+1}} = \frac{\partial \bar{\sigma}_{n+1}}{\partial \boldsymbol{\varepsilon}_{n+1}^{etrial}}. \tag{54}$$

In order to give the linear tangent relationship between $\boldsymbol{\varepsilon}_{n+1}^{e\,trial}$ and $\boldsymbol{\sigma}_{n+1}$, we linearize the nonlinear system $\{\mathbf{f}(\mathbf{x})\} = \{\mathbf{0}\}$, including the elastic trial strain as a variable. The differentiation of the nonlinear system can be expressed as

$$\begin{bmatrix} \mathbf{Q} & \mathbf{M} \\ \mathbf{N} & \mathbf{U} \end{bmatrix} \begin{Bmatrix} \mathrm{d}\boldsymbol{\sigma} \\ \mathrm{d}\mathbf{X} \end{Bmatrix} = \begin{Bmatrix} \mathrm{d}\boldsymbol{\varepsilon}_{n+1}^{etrial} \\ \mathbf{0} \end{Bmatrix}, \tag{55}$$

where

$$\{\mathrm{d}\mathbf{X}\} = \left\{\mathrm{d}\boldsymbol{\chi}_{n+1}^t, \mathrm{d}\boldsymbol{\chi}_{n+1}^p, \mathrm{d}\Delta\lambda^t, \mathrm{d}\Delta\lambda^p, \mathrm{d}\gamma_{n+1}\right\}, \tag{56}$$

$$\{\mathbf{M}\} = \left\{\Delta\lambda^t \frac{\partial \mathbf{N}^t}{\partial \boldsymbol{\chi}^t}, \quad \Delta\lambda^p \frac{\partial \mathbf{N}^p}{\partial \boldsymbol{\chi}^p}, \quad \mathbf{N}^t, \quad \mathbf{N}^p, \quad \mathbf{0}\right\}, \tag{57}$$

$$\{\mathbf{N}\} = \left\{-\Delta\lambda^t \mathbf{P} : \frac{\partial \mathbf{N}^t}{\partial \boldsymbol{\sigma}}, \quad -\tfrac{2}{3} C^p \Delta\lambda^p \frac{\partial \mathbf{N}^p}{\partial \boldsymbol{\sigma}}, \quad \mathbf{N}^t, \quad \mathbf{N}^p, \quad \Delta\lambda^t \frac{\partial \mathbf{N}^t}{\partial \boldsymbol{\sigma}} : \mathbf{N}^{\boldsymbol{\varepsilon}^t}\right\}^T, \tag{58}$$

$$[\mathbf{U}] = \begin{bmatrix} \mathbf{I} - \Delta\lambda^t \mathbf{P} : \frac{\partial \mathbf{N}^t}{\partial \boldsymbol{\chi}^t} & \mathbf{0} & -\mathbf{P} : \mathbf{N}^t & Q'(p)\mathbf{N}^{\boldsymbol{\varepsilon}^t} & -\mathbf{N}^{\boldsymbol{\varepsilon}^t} \\ \mathbf{0} & \mathbf{I} - \tfrac{2}{3} C^p \Delta\lambda^p \frac{\partial \mathbf{H}^p}{\partial \boldsymbol{\chi}^p} & \mathbf{0} & -\tfrac{2}{3} C^p \mathbf{H}^p & \mathbf{0} \\ -\mathbf{N}^t & \mathbf{0} & 0 & 0 & 0 \\ m\Delta\lambda^t \frac{\partial \mathbf{N}^t}{\partial \boldsymbol{\chi}^t} : \mathbf{N}^{\boldsymbol{\varepsilon}^t} & -\mathbf{N}^p & m\mathbf{N}^{\boldsymbol{\varepsilon}^t} : \mathbf{N}^t & -R'(p) & 0 \\ \Delta\lambda^t \frac{\partial \mathbf{N}^t}{\partial \boldsymbol{\chi}^t} : \mathbf{N}^{\boldsymbol{\varepsilon}^t} & 0 & \mathbf{N}^{\boldsymbol{\varepsilon}^t} : \mathbf{N}^t & 0 & 0 \end{bmatrix}. \tag{59}$$

The increment of stress can be computed with

$$\Delta\boldsymbol{\sigma}_{n+1} = \left[\mathbf{Q} - \{\mathbf{M}\} : [\mathbf{U}]^{-1} : \{\mathbf{N}\}\right]^{-1} : \Delta\boldsymbol{\varepsilon}_{n+1}^{e\,trial}, \tag{60}$$

then the consistent tangent operator can be obtained as

$$\mathbf{D}^{in} = \left[\mathbf{Q} - \{\mathbf{M}\} : [\mathbf{U}]^{-1} : \{\mathbf{N}\}\right]^{-1}. \tag{61}$$

4 Application and Verification

4.1 Pseudoelasticity and shape memory effect

The shape memory alloy adopted in this subsection is the same as that by Panico and Brinson (2007). M_f, M_s, A_s and A_f were given as 306K, 310K, 317K and 319K, respectively. Neglecting the insignificant plastic deformation during the processes related to pseudoelasticity and shape memory effect, the relative material constants are identified and listed in Table 1.

Table 1: Material constants of an SMA [Panico and Brinson (2007)]

E (GPa)	ν	B (MPa /K)	M_0 (K)	C^t (MPa)	σ^t(MPa)	ε_L
68.4	0.36	14.2	310	300	100	0.047

Figure 1 shows the pseudoelastic tensile stress-strain curve of the material at T=325K. The constitutive behavior of the shape memory alloys is pseudoelastic since $T > A_f$.. It can be seen that the martensitic transformation strain induced by the applied stress is totally recovered without considering the impact of plastic deformation.

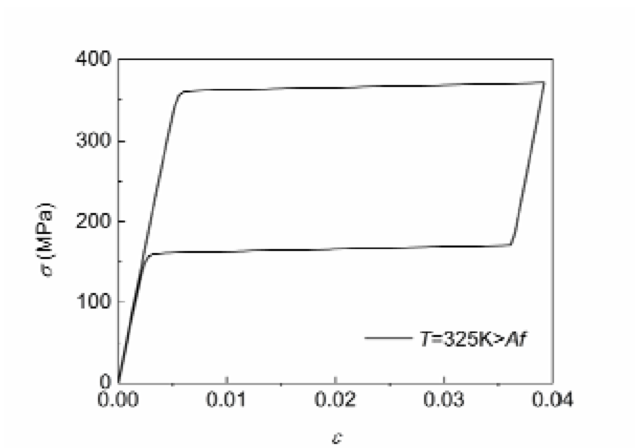

Figure 1: Pseudoelastic behavior at T=325K

Figure 2 shows the shape memory effect of the material. The material undergoes tensile loading and unloading at martensitic transformation starting temperature Ms (T=310K), followed by heating to T=320K. It is known that during the loading and unloading process, the material should mainly be martensite, and the deformation due to the detwinning of martensite variants remains after unloading. During the following heating, the inverse transformation takes place once $T > A_s$, and develops with the increase of temperature until $T = A_f$ when the material returns completely to its parent phase. The transformation strain recovers with the increase of temperature, and disappears as T=A_f. Noticing that the values of A_s and A_f are 317K and 319K, but the calculated results is only about 315K and 316K, which may be accounted for with that the transformation strain by detwinning affects the value of the back stress, then affects the inverse transformation temperature. It can be seen that the typical characteristics of pseudoelasticity and shape memory effect of the SMA can be described reasonably with the proposed model.

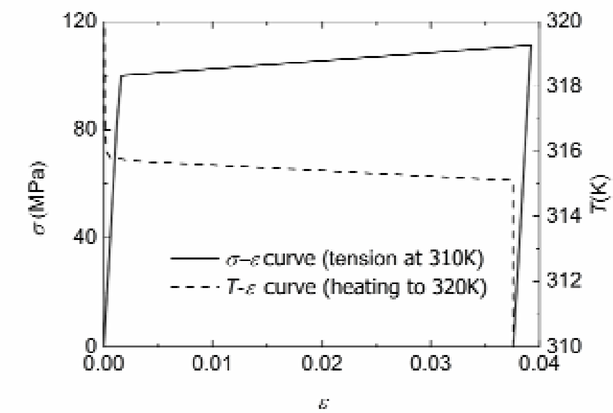

Figure 2: Shape memory effect (Tension at T=310K, then unloading followed by heating to T=320K)

4.2 Effect of plastic deformation on transformation

Wang et al. (2008) studied the effect of plastic deformation on the pseudo-elastic behavior of an NiTi SMA at room temperature. The stress responses at different strain amplitudes were presented (Fig. 3). It was found that the hysteretic loop of the σ - ε curves increases if plastic strain occurs, implying that plastic strain can impede the inverse transformation.

Since the deformation takes place at a constant temperature, the effects of temperature on the material properties, the strain induced by thermal expansion and the corresponding stress are not taken into account. Making use of the experimental curve corresponding to ε_{max}=0.06, the material constants related to elastic and transformation deformation can be identified; then the material constants related to plastic deformation and its effects on transformation can be identified with a stress-strain curve involving plastic deformation, for example, the curve corresponding to ε_{max}=0.10. The material constants identified are listed in Table 2.

Table 2: Material constants of an NiTi SMA [Wang et al. (2008)]

E (GPa)	ν	B (MPa / ^{o}C)	M_0 (^{o}C)	C^t (MPa)	C^p (MPa)	ξ	ζ
57	0.3	5.65	-29.2	300	500	15	15
Y_0 (MPa)	R_0 (MPa)	Q_0 (MPa)	σ_s^t(MPa)	σ_s^p (MPa)	a	ε_L	θ (1/K)
100	210	300	85.5	550	0	0.068	0

The responses of the SMA subjected to tensile deformation to different strain amplitudes are analyzed and shown in Fig. 4. Compared with the experimental results, it can be seen that the main characteristics of the material can be reasonably described. Distinct martensitic transformation starts at $\varepsilon \approx 0.004$, then the stress of the material is mainly determined by the martensitic transformation due to the detwinning of the martensite variants. The forward transformation or detwinning continues until $\varepsilon \approx 7.2\%$. Then the resistance against the further straining increases due to plastic deformation. Marked plastic strain induced hardening can be observed (Fig. 4), which can also be described reasonably with the proposed model. At the onset of unloading, the response of the material is mainly determined by the elastic property of the martensite. With the decrease of stress, the resistance against inverse transformation is released, and inverse transformation may occur when the resistance decreases to a criterion determined by the previous plastic strain amplitude. It can be seen that the inverse transformation during unloading should occur at a high level of stress if the previous maximum strain $\varepsilon_{max} \approx 7.2\%$ (Fig. 4) when no plastic deformation takes place.

It can also be seen that with the increase of the plastic strain, the stress corresponding to the inverse transformation decreases monotonically, indicating a larger hysteresis loop compared with that without taking into account the effect of plastic deformation [Peng et al. (2012)], which implies that more strain energy will be dissipated in the inverse transformation process. A reasonable explanation is that plastic deformation dissipates or releases the elastic energy stored in the material during a deformation process, therefore, additional energy should be needed for the inverse transformation of the material. It can also be observed that the residual strain after unloading is almost the plastic strain that occurred during the previous loading process. All these characteristics can be reasonably replicated with the proposed model.

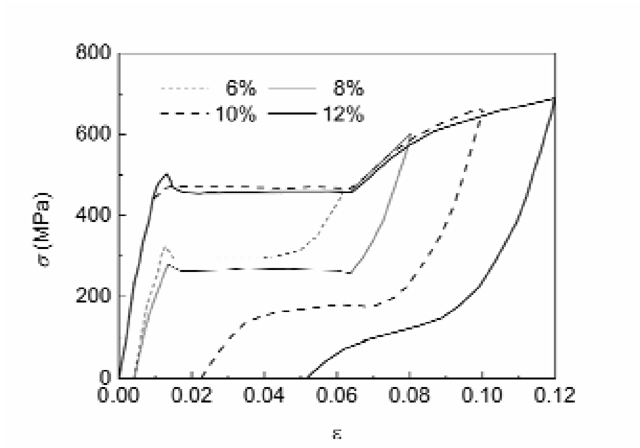

Figure 3: σ - ε curves of an SMA subjected to different strain amplitudes

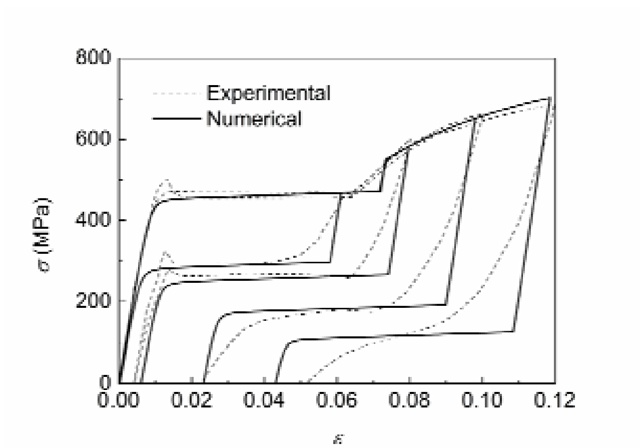

Figure 4: Experimental and computed σ - ε curves at different strain amplitudes

Piao et al. (1993) also investigated the origin for the increase of A_s of a kind of $Ti_{49.5}Ni_{50.5}$ polycrystalline alloy at room temperature by pre-deformation, and found that the increase of A_s is closely related to the permanent strain. Miyazaki et al. (1981) divided a stress-strain curve in to three stages (Fig. 5): (I) The initial linear part corresponding to elastic deformation, followed by a plateau corresponding to stress-induced martensitic transformation, where the transformation strain increases, indicating the occurrence of the stress-induced transformation, detwinning or twinning to more favorable orientations with increasing stress; (II) A rapid strain hardening induced by permanent strain due to slip; and (III) The strain hardening tends to saturation and the recoverable strain decreases. The material used by Piao et al. (1993) is adopted in this subsection and the material constants are identified and listed in Table 3.

Figure 5 shows the experimental and computed σ-ε curves of the $Ti_{49.5}Ni_{50.5}$ alloy at T =298K, lying between M_s=289K and A_s=307K. The computed result implies that the proposed model can replicate the main characteristics of the SMA subjected to large tensile deformation. It should be noted that ε_L=0.085 is adopted based on the assumption that transformation and slip take place simultaneously.

Table 3: Material constants of $Ti_{49.5}Ni_{50.5}$ [Piao et al. (1993)]

E (GPa)	ν	B (MPa / ^oC)	M_0 (^oC)	C^t (MPa)	C^p (MPa)	ξ	ζ
27.4	0.3	6.10	289	300	300	55	8
Y_0 (MPa)	R_0 (MPa)	Q_0 (MPa)	σ_s^t(MPa)	σ_s^p (MPa)	a	ε_L	θ(1/K)
2300	200	200	120	450	0	0.085	0

In order to verify the effect of the pre-deformation on A_s, we simulate the SME of the SMA subjected to straining of different amplitudes at 298K, then unloading followed by heating for inverse transformation. Figure 6 shows the computed shape memory effect of the SMA. It can be seen that different residual strain remains after unloading. During heating, the residual strain keeps unchanged until the temperature reaches a critical value, A_s, then part of it recovers with the increase of temperature, and some irrecoverable part remains even if the temperature increases to over A_f(the dashed lines). It can be seen that both A_s and $A_f$increase with the increase of the irreversible deformation and tend to be saturated, indicating that more energy is needed during the inverse transformation to compensate for that dissipated by irreversible deformation.

Figure 7 shows the evolutionary character of the $Ti_{49.5}Ni_{50.5}$ alloy under constrained recovery condition. The specimen is firstly stretched to ε_{max}=0.15 and unloaded at 298K, then the two ends of the specimen are fixed and the specimen is subjected to

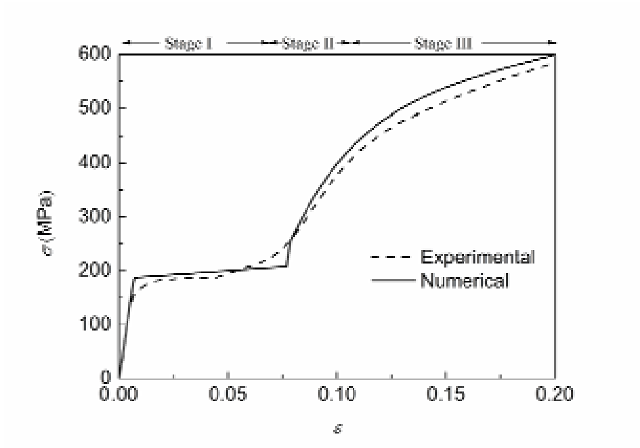

Figure 5: Experimental and computed σ-ε curves at room temperature (298K)

a temperature cycle, as shown in Fig. 7. The variation of stress against temperature is shown in Fig. 7, where the contribution by thermal expansion has been excluded. It can be seen that the stress almost undergoes a cycle during a temperature loop, similar to the experimental observation of SMA $Ti_{50}Ni_{45}Cu_5$[Šittner et al. (2000)].

If ΔA_s denotes the increase in the austenite transformation start temperature, its saturation value $(\Delta A_s)_{max}$ can easily be evaluated with $(\Delta A_s)_{\max} = Q_0/B$ by using Equation (11). The comparison of the computed $\Delta A_s \sim \varepsilon_p$ curve with the experimental one is shown in Fig. 8, where it can be seen that the proposed model can satisfactorily describe the experimental result.

We now discuss the mechanism of the variation of ΔA_s against increasing irreversible deformation. It can be found in Equations (11) and (19) that $Q(p)$ affects directly the conditions for the occurrence of transformation. When plastic deformation occurs, in order for the inverse transformation to occurs, the system needs a higher temperature or lower level of stress. Piao et al. (1993) proposed a clearer mechanism for this phenomenon by focusing the attention on the stored elastic energy in thermoelastic alloys, which can be used in the following inverse transformation. If plastic deformation dissipates this part of energy, additional energy should be supplied in the following inverse transformation for compensation by either increasing inverse transformation start temperature (thermal energy) or decreasing the applied stress level, which results in a larger area of the hysteretic loop, indicating more energy are absorbed during the inverse transformation.

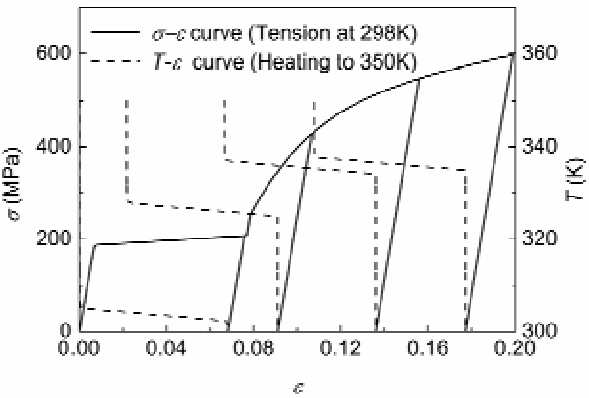

Figure 6: Shape memory effect of SMA subjected to different tensile deformation (Stretched at 298K to the prescribed strain, unloaded, and then heated to 350K

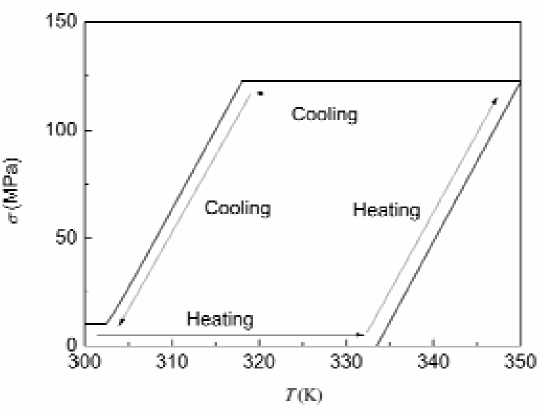

Figure 7: Evolutionary character of SMA under constrained recovery condition

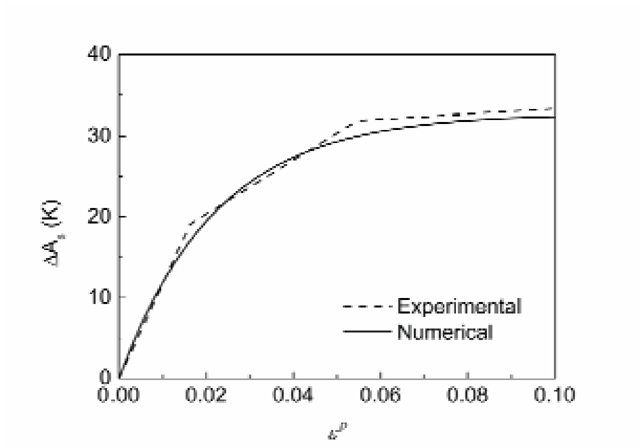

Figure 8: Variation of ΔA_s against ε^p

The incomplete recovery of the stress-induced transformation strain was found in the experiments on alloy Ti–50.9at%Ni subjected to cyclic loading at T=319K [Strnadel et al.(1995)], which leads to a small residual strain remaining after unloading. The material constants of alloy Ti–50.9at%Ni are identified with the experimental results and listed in Table 4.

Table 4: Material constants of alloy Ti–50.9at%Ni [Strnadel et al.(1995)]

E (GPa)	ν	B (MPa / ^{o}C)	M_0 (^{o}C)	C^t (MPa)	C^p (MPa)	ξ	ζ
46.0	0.33	4.10	243	500	10000	0	0
Y_0 (MPa)	R_0 (MPa)	Q_0 (MPa)	σ_s^t(MPa)	σ_s^p (MPa)	a	ε_L	θ (1/K)
0	0	0	116	500	0	0.058	0

Figure 9 shows the experimental and the computed σ-ε curves at 319K, where the proposed model describes reasonably the stress induced transformation and permanent deformation.

4.3 Responses of SMAs under biaxial loadings

McNaney et al. (2003) performed the tension–torsion experiments on thin-walled superelastic Nitinol tubes, and found significantly different characteristics from those under uniaxial loading, which are to be simulated with the proposed model. The material constants are identified with the torsional experimental result by McNaney et al. (2003) and listed in Table 5.

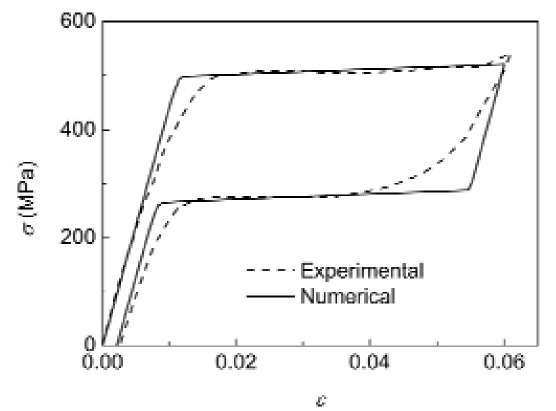

Figure 9: Experimental and computed σ-ε curves of Ti–50.9 at%Ni at 319K

Table 5: Material constants of superelastic Nitinol [McNaney et al. (2003)]

E (GPa)	ν	B (MPa / ^{o}C)	M_0 (^{o}C)	C^t (MPa)	C^p (MPa)	ξ	ζ
36.0	0.33	2.2	184.87	1000	0	0	0
Y_0 (MPa)	R_0 (MPa)	Q_0 (MPa)	σ_s^t(MPa)	σ_s^p (MPa)	a	ε_L	θ (1/K)
0	0	0	135	∞	0	0.061	0

Figure 10 (a) shows a biaxial strain path in the$\varepsilon - \gamma/\sqrt{3}$ plane, and Fig. 10 (b) demonstrates comparison between the experimental and the computed σ_{eq}- ε_{eq} curves by this path, where σ_{eq} and ε_{eq} denote equivalent stress and equivalent strain, respectively. It can be seen in Fig. 10 (b) that the computed σ_{eq} to the straining part AB over predicts the experimental result, which could be attributed to the marked difference between the responses under pure tension and under pure torsion due to the marked difference between the corresponding microstructures of this kind of materials (Peng et al, 2008), and the material constants that were identified with the torsional experimental result may over predict the stress under tensile staining. The response of the material at larger strain amplitude is also computed. The comparison between the computed and the experimental result shows that the main characteristic of the material under the biaxial strain path can reasonably be replicated.

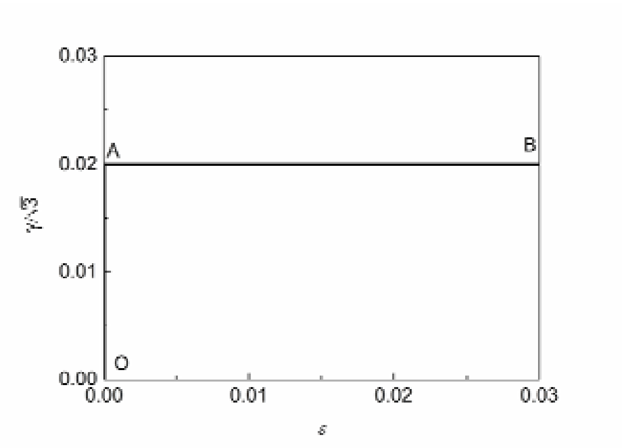

(a)

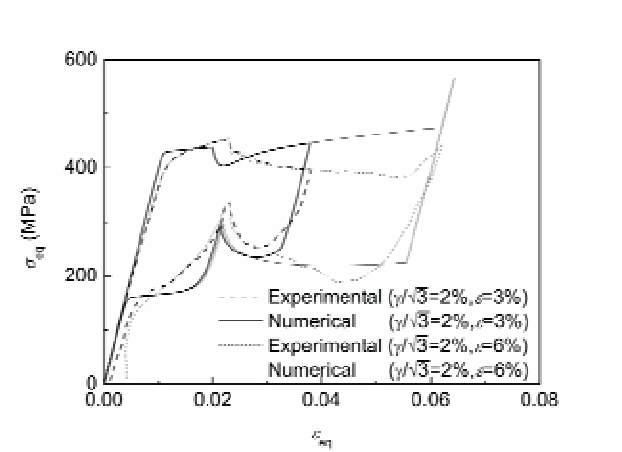

(**b**)

Figure 10: Biaxial strain response path and stress response (a) Biaxial strain path (O→A→B→A→O) (b) Comparison between computed and experimental results

4.4 An application

Because of the unique shape memory effect, reliable performance, convenient installation and the other distinct advantages, SMA pipe joints have been used in many important cases. The installation of an SMA pipe joint is simulated in this subsection in a general way using the finite element method (FEM).

Figure 11: FEM mesh of a SMA pipe joint

The constitutive behavior of SMAs is described with a return-mapping algorithm, the implementation of the model into the finite element code ABAQUS/Standard through a User MATerial subroutine (UMAT) has been discussed in Section 3. Figure 11 shows the finite element mesh of the pipe joint and the pipes to be connected, where element type C3D8 (an 8-node linear brick element) is adopted. The inner and outer diameters of the pipe are 15 and 30 mm, respectively. In order to study the variation of contact pressure against plastic deformation, the installations of the pipe joints with five different inner diameters, 28.0, 28.4, 28.8, 29.2 and 29.6 mm, are simulated respectively. The thickness of the pipe joint is 10 mm. Before installation, the inner diameter of each joint is reamed to 31.2 mm at a low temperature (T=289K), then assembled on the pipes to be connected, then it is heated to T=350K (above the A_f taking into account the increase by plastic deformation), and at last it is cooled to room temperature. The material with the properties listed in Table 3 is adopted for joint material, keeping in mind M_s=289K and A_s=307K. The material of the steel pipes is assumed elastoplastic with the Young's modulus E=205GPa, the Poisson's ratioν=0.28, and the yield stress σ_s=454MPa, and the ultimate stress σ_p=790MPa, respectively. In order to focus on the transformation behavior, the effect of thermal expansion is excluded from the analysis.

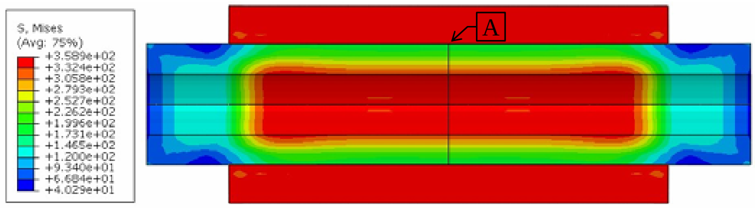

(a)

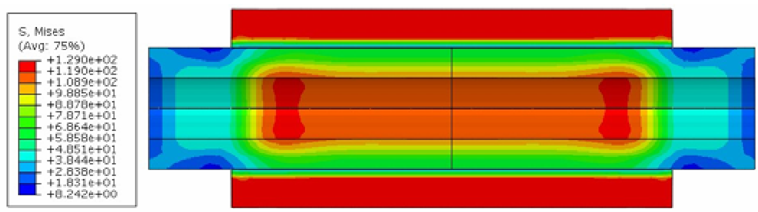

(b)

Figure 12: Distribution of σ_{eq} in pipe-joint with inner diameter 28.4 mm (a) after heated to 350 K, (b) after being cooled to room temperature

Figure 12 (a) shows the distribution of σ_{eq} in the pipe-joint system with inner diameter 28.4 mm after heated to 350 K. Figure 12(b) shows the distribution of equivalent stress in the assembled pipe-joint system after being cooled to room temperature. Figure 13 shows the variation of circumferential strain ε_{22} and stress σ_{22} during the installation process at point A marked in Fig. 12(a). It can be seen that the strain in the SMA pipe joint start to recover when the temperature is increased to about 308 K attributed to a little plastic strain generate in the material. With increasing temperature, the joint contracts and contacts the pipes, and the stress in the joint increases rapidly. The variation of σ_{22} in the joint and the contact pressure, p, with decreasing temperature at point A are shown in Fig 14.

Figure 15 shows the variation of interfacial contact pressure p against temperature in the area A, with different inner diameters of the joint, d_{in}, as a parameter. It can be seen that the temperature for the joint of d_{in} =28 mm to start contacting the pipes is about 310 K, it decreases slightly with the increase of d_{in}. p increases

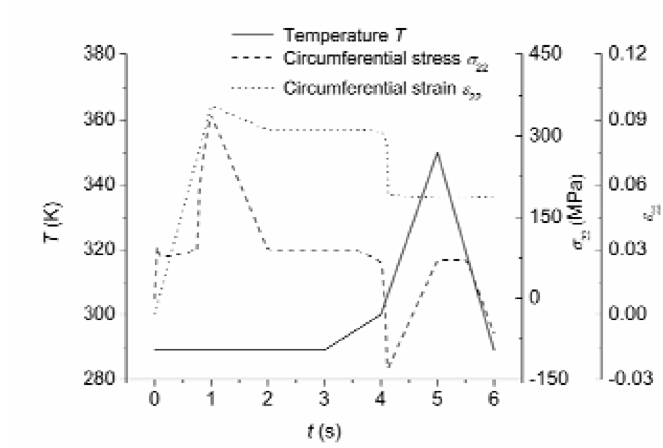

Figure 13: Variations of several variables in assembly process

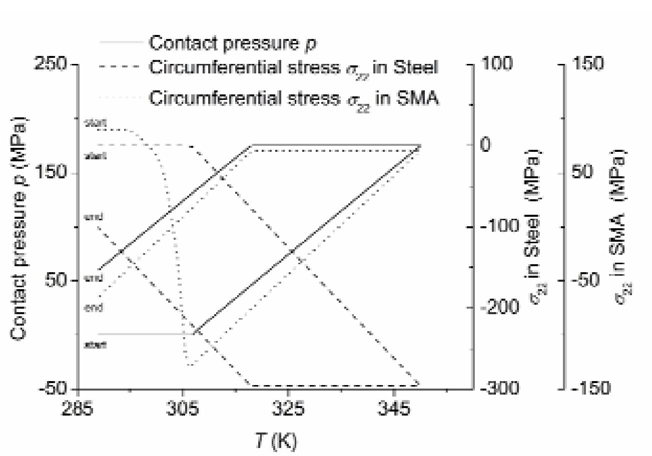

Figure 14: Variations of σ_{22} and p against T at point A

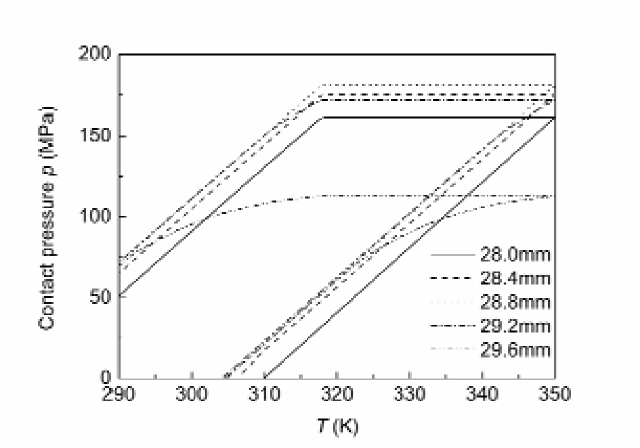

Figure 15: Variations of p against T, with d_{in} of joint as a parameter at point A

rapidly with the increase of T because of inverse transformation. During cooling, the stress keeps constant (without considering the effect of thermal expansion) until the onset of martensitic transformation. Then p decreases with the development of martensitic transformation until T falls to room temperature.

Figure 16 shows the variation of the contact pressure$p$ near Point A at 350 K and the contact pressure after cooled to room temperature, corresponding to the joints of different initial diameters. It can be seen that after installation the contact pressure between the joint and the pipes is sufficient to prevent from leakage. The recovered strain, ε_{re}, corresponding to different d_{in} of the joint is also shown in Fig. 16, which is defined as that the strain recovered in the joint after the joint contacts pipes. It can be seen that the contact pressure at 350 K is almost proportional to the recovered strain. With the increase of d_{in}, the contact pressure p at 350K increases at first and then decreases. When the inner diameter d_{in} of all joints is reamed to 31.2 mm, the joint with smaller initial inner diameter will suffer larger inelastic deformation, including not only larger recoverable deformation, but also larger plastic deformation. Too small initial inner diameter may result in severe plastic deformation and reduces the recoverable capability of the joint. On the other hand, too large initial inner diameter may also result in insufficient recoverable capability because of the induced too small recoverable strain. Thus, there is an optimal d_{in}that may result in satisfactory both plastic and recoverable deformation, and generates satisfactory contact pressure. The comparison between the contact pressures corresponding to different initial inner diameters of the joint 28.8mm $\leq d_{in} \leq$ 29.6mm may result in satisfactory contact pressure.

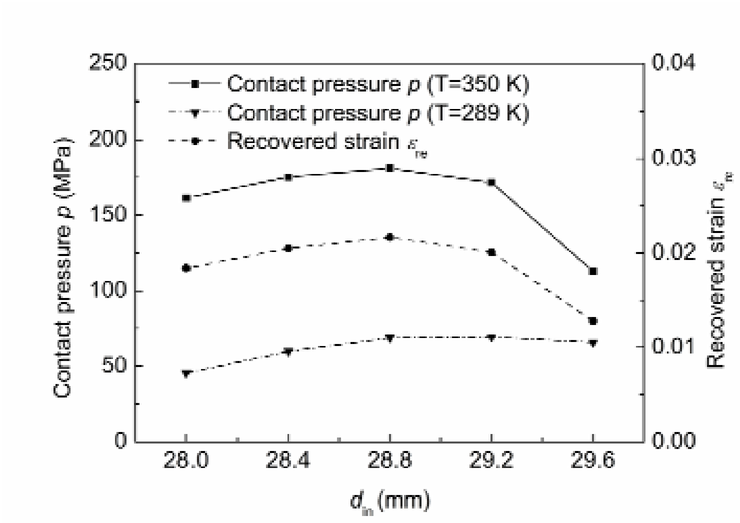

Figure 16: p and ε_{re} at 350K and 289K, corresponding to different d_{in} of joint

5 Conclusions

In this article, we proposed a three-dimensional constitutive model for shape memory alloys, considering plastic deformation and its effects. Making use of a free energy function and following the conventional procedure, we derived the driving force for the phase transformation and that for the plastic deformation. Two yield functions are defined to describe the phase transformation and the plastic deformation, respectively. The corresponding integration algorithm was obtained, including stress updating algorithm and the tangent stiffness expression. The typical characteristics of SMAs and the effects of plastic deformation are analyzed. The typical properties of SMAs, such as shape memory effect and pseudoelasticity can be described with the model without taking into account plastic deformation. As a simple application, the installation process of a SMA pipe joint was simulated, which demonstrates the validity of the proposed model and the corresponding numerical approach.

Acknowledgement: The authors gratefully acknowledge the financial support to this work from NSFC under Grant Number 10976032 and 11272364.

References

Auricchio, F.; Taylor, R.L.; Lubliner, J. (1997): Shape memory alloys: macromodelling and numerical simulations of the superelastic behavior. *Comput. Method Appl. Mech. Eng.,* vol.146, pp.281–312.

Auricchio, F.; Petrini, L.; (2002): Improvements and algorithmical considerations on a recent three-dimensional model describing stress-induced solid phase transformations. *Int. J. Numer. Method Eng.*, vol.55 (11), pp.1255–1284.

Auricchio, F.; Petrini, L. (2004a): A three-dimensional model describing stress-temperature induced solid phase transformations: solution algorithm and boundary value problems. *Int. J. Numer. Method Eng.,* vol.61, pp.807–836.

Auricchio, F.; Petrini, L. (2004b): A three-dimensional model describing stress-temperature induced solid phase transformations: thermomechanical coupling and hybrid composite applications. *Int. J. Numer. Method Eng*., vol.61, pp.716–737.

Auricchio, F.; Reali, A.; Stefanelli, U. (2007): A three-dimensional model describing stress-induced solid phase transformation with permanent inelasticity. *Int. J. Plasticity,* vol.23, pp.207–226.

Auricchio, F.; Conti, M.; Morganti, R.A. (2010): Shape memory alloy: from constitutive modeling to finite element analysis of stent deployment. *CMES: Computer Modeling in Engineering & Sciences*, vol.57(3), pp.225–243.

Arghavani, J.; Auricchio, F. Naghdabadi, R.; Reali, A.; Sohrabpour, S (2010): A 3-D phenomenological constitutive model for shape memory alloy under multiaxial loadings. *Int. J. Plasticity,* vol.26, pp.976–991.

Blanc, P.; Lexcellent, C. (2004): Micromechanical modelling of a CuAlNi shape memory alloy behaviour. *Mater. Sci. Eng. A,* vol.378, pp.465–469.

Bo, Z.H.; Lagoudas, D.C. (1999a): Thermomechanical modeling of polycrystalline SMAs under cyclic loading, Part I: theoretical derivations. *Int. J. Eng. Sci.*, vol.37, pp.1089–1140.

Bo, Z.H.; Lagoudas, D.C. (1999b): Thermomechanical modeling of polycrystalline SMAs under cyclic loading, Part III: evolution of plastic strains and two-way shape memory effect. *Int. J. Eng. Sci.,* vol.37, pp.1175–1203.

Bo, Z.H.; Lagoudas, D.C. (1999c) Thermomechanical modeling of polycrystalline SMAs under cyclic loading, Part IV: modeling of minor hysteresis loops. *Int. J. Eng. Sci.,* vol.37, pp.1205–1249.

Boyd, J.G.; Lagoudas, D.C. (1996): A thermodynamic constitutive model for the shape memory materials. Part I. The monolithic shape memory alloys. *Int. J. Plasticity,* vol.12 (6), pp.805–842.

Brinson, L., C. (1993): One-dimensional constitutive behavior of shape memory alloys: thermomechanical derivation with non-constant material functions and redefined martensite internal variable. *J. Intel. Mat. Syst. Struct.,* vol.4(2), pp.229–242.

Casciati, F.; Casciati, S.; Faravelli, L.; Marzi, A. (2011): Fatigue damage accumulation in a Cu-based shape memory alloy: preliminary investigation. *CMC: Computers, Materials & Continua*, vol. 23(3), pp. 287-306.

Entchev, P.B.; Lagoudas, D.C. (2002): Modeling porous shape memory alloys using micromechanical averaging techniques. *Mech. Mater.,* vol.34, pp.1–24.

Frémond, M. (1987): Shape memory alloys. *CR. ACAD. SCI. II.* vol.304, pp.239-246.

Frémond, M.; Nedjar, B. (1996): Damage, gradient of damage and principle of virtual power. *Int. J. Solids Struct.,* vol.33, pp.1083-1103.

Gao, X.J.; Huang, M.; Brinson, L.C. (2000a): A multivariant micromechanical model for SMAs Part 1. Crystallographic issues for single crystal model. *Int. J. Plasticity,* vol.16, pp.1345–1369.

Gao, X.J.; Huang, M.; Brinson, L.C. (2000b): A multivariant micromechanical model for SMAs Part 2.Polycrystal model. *Int. J. Plasticity,* vol.16, pp.1371–1390.

Helm,D.; Haupt, P. (2003): Shape memory behaviour: modelling within continuum thermomechanics. *Int. J. Solids Struct.,* vol.40, pp.827–849.

Hartl, D.J.; Lagoudas, D.C. (2009): Constitutive modeling and structural analysis considering simultaneous phase transformation and plastic yield in shape memory alloys. *Smart Mater. Struct.,* vol.18, pp.104017

Hartl, D.J.; Chatzigeorgiou, G.; Lagoudas, D.C. (2010): Three-dimensional modeling and numerical analysis of rate-dependent irrecoverable deformation in shape memory alloys. *Int. J. Plasticity,* vol.26(10), pp.1485–1507.

Jemal, F.; Bouraoui, T.; Zine, T.B.; Patoor, E.;Bradaï, C. (2009): Modelling of martensitic transformation and plastic slip effects on the thermo-mechanical behaviour of Fe-based shape memory alloys. *Mech. Mater.,* vol.41, pp.849–856.

Kang, M.K.; Kim, E.H.; Rim, M.S.; Lee, I. (2010): Engineering model to predict behaviors of shape memory alloy wire for vibration applications, *CMES: Computer Modeling in Engineering & Sciences*, vol. 64(3), pp. 227-250.

Lagoudas, D.C.; Bo, Z.H. (1999): Thermomechanical modeling of polycrystalline SMAs under cyclic loading, Part II: material characterization and experimental results for a stable transformation cycle. *Int. J. Eng. Sci.,* vol.37, pp.1141–1173.

Lagoudas, D.C.; Entchev, P.B.; Popov, P., Patoor, E.; Brinson, L.C.; Gao, X.J. (2006): Shape memory alloys, Part II: Modeling of polycrystals. *Mech. Mater.,* vol.38, pp.430–462.

Leclercq, S.; Lexcellent, C. (1996): A general macroscopic description of the thermomechanical behavior of shape memory alloys. *J. Mech. Phys. Solids,* vol.44(6), pp.953–957.

Lemaitre, J.; Chaboche, J.L. (1990): Mechanics of Solids Materials. *Cambridge University Press.*

Lexcellent, C.; Goo, B.C.; Sun, Q.P.; Bernardini, J. (1996): Characterization thermomechanical behaviour and micromechanical-based constitutive model of shape-memory Cu-Zn-Al single crystals. *Acta Mater.,* vol.44(9), pp.3773–3780.

Lexcellent, C.; Goo, B.C. (1997): Micromechanics-based modeling of two-way memory effect of a single crystalline shape-memory alloy. *Acta Mater.,* vol.45(2), pp.127–137.

Liang, C.; Rogers, C.A. (1990): One-dimensional thermomechanical constitutive relations for shape memory materials. *J. Intel. Mat. Syst. Struct.,* vol.1(2), pp.207–234.

Liu, B.; Dui, G; Zhu, Y. (2011): A constitutive model for porous shape memory alloys considering the effect of hydrostatic Stress, *CMES: Computer Modeling in Engineering & Sciences*, vol. 78(4), pp. 247-276.

McNaney, J.M.; Imbeni, V. et al. (2003): An experimental study of the superelastic effect in a shape-memory Nitinol alloy under biaxial loading. *Mech. Mater.,* vol.35, pp.969–986.

Miyazaki, S.; Otsuka, K.; Suzuki, Y. (1981): Transformation pseudoelasticity and deformation behavior in a Ti-50.6 at % Ni alloy. *Scripta Mater.,* vol.15, pp.287–292.

Paiva, A.; Savi, M.; A. et al. (2005): A constitutive model for shape memory alloys considering tensile–compressive asymmetry and plasticity. *Int. J. Solids Struct.,* vol.42, pp.3439–3457.

Panico, M.; Brinson, L.C. (2007): A three-dimensional phenomenological model for martensite reorientation in shape memory alloys. *J. Mech. Phys. Solids,* vol.55, pp.2491–2511.

Patoor, E.; Lagoudas, D.C.; Entchev, P., B.; Brinson, L.C.; Gao, X.J. (2006): Shape memory alloys, Part I: General properties and modeling of single crystals. *Mech. Mater.,* vol.38, pp.391–429.

Peng, X.; Yang, Y.; Huang, S. (2001): A comprehensive description for shape memory alloys with a two-phase constitutive model. *Int. J. Solids Struct.,* vol.38, pp.6925–6940.

Peng, X.; Chen, B.; Chen, X.; Wang, J.; Wang H. (2012): A constitutive model for transformation, reorientation and plastic deformation of shape memory alloys, *Acta Mech. Solida Sinica*, vol. 25, pp285-298.

Peng, X.; Pi, W.; Fan, J. (2008): A microstructure-based constitutive model or the pseudoelastic behavior of NiTi SMAs. *Int. J. Plasticity,* vol.24, pp.966–990.

Piao, M.; Otsuka, K.; Miyazaki, S.; Horikawa, H. (1993): Mechanism of the As temperature increase by pre-deformation in thermoelastic alloys. *Mater. Trans., JIM*, vol.34(10), pp.919–929.

Popov, P.; Lagoudas, D.C. (2007): A 3-D constitutive model for shape memory alloys incorporating pseudoelasticity and detwinning of self-accommodated martensite. *Int. J. Plasticity,* vol.23, pp.1679–1720.

Raniecki, B.; Lexcellent, C. (1998): Thermodynamics of isotropic pseudoelasticity in shape memory alloys. *Eur. J. Mech. A-Solid,* vol.17, pp.185–205.

Siredey, N.; Patoor, E.; Berveiller, M.; Eberhardt, A. (1999): Constitutive equations for polycrystalline thermoelastic shape memory alloys. Part I. Intragranular interactions and behavior of the grain. *Int. J. Solids Struct.,* vol.36, pp.3178–3204.

Souza, A.C.; Mamiya E.N.; Zouain, N. (1998): Three-dimensional model for solids undergoing stress-induced phase transformations. *Eur. J. Mech. A-Solid,* vol.17, pp.789–806.

Strnadel, B.; Ohashi, S.; Ohtsuka, H.; Miyazaki, S.; Ishihara, T. (1995): Effect of mechanical cycling on the pseudoelasticity characteristics of Ti–Ni and Ti–Ni–Cu alloys. *Mater. Sci. Eng. A,* vol.203, pp.187–196.

Sun, Q.P.; Hwang, K.C. (1993a): Micromechanics modeling for the constitutive behavior of polycrystalline shape memory alloys – I. Derivation of general relations. *J. Mech. Phys. Solids,* vol.41 (1), pp.1–17.

Sun, Q.P.; Hwang, K.C. (1993b): Micromechanics modeling for the constitutive behavior of polycrystalline shape memory alloys – II. Study of the individual phenomena. *J. Mech. Phys. Solids,* vol.41 (1), pp.19–33.

Šittner, P.; Vokoun, D.; Dayananda, G.; Stalmans, R. (2000): Recovery stress generation in shape memory $Ti_{50}Ni_{45}Cu_5$ thin wires. *Mater. Sci. Eng. A,* vol.286 (2), pp.298–311.

Tanaka, K.; Nishimura, F.; Hayashi, T.; Tobushi, H.; Lexcellent, C. (1995): Phenomenological analysis on sub loops and cyclic behavior in shape memory alloys under mechanical and/or thermal loads. *Mech. Mater.,* vol.19, pp.281–292.

Wang, X.M.; Xu, B,X.; Yue, Z.F. (2008): Phase transformation behavior of pseudoelastic NiTi shape memory alloys under large strain. *J. Alloys Compounds,* vol.463, pp.417–422.

Zaki, W.; Moumni, Z. (2007): A 3D model of the cyclic thermomechanical behavior of shape memory alloys. *J. Mech. Phys. Solids,* vol.55, pp.2427–2454.

Zaki W.; Zamfir, S.; Moumni, Z. (2010): An extension of the ZM model for shape memory alloys accounting for plastic deformation. *Mech. Mater.,* vol.42, pp.266–274.

Zhao, L.C.; Zhang, C.S. (1992): Proceedings of the Conference on Martensitic Transformations. Monterey: Monterey Institute for Advanced Studies.